Eur. Phys. J. C (2024) 84:1240
https://doi.org/10.1140/epjc/s10052-024-13500-3

THE EUROPEAN PHYSICAL JOURNAL C

Regular Article

Theoretical Physics

Rotating charged black holes in EMS theory: shadow studies and constraints from EHT observations

Odil Yunusov[1,a], **Javlon Rayimbaev**[2,3,4,b], **Furkat Sarikulov**[1,5,c], **Muhammad Zahid**[6,d], **Ahmadjon Abdujabbarov**[7,8,9,e], **Zdeněk Stuchlík**[10,f]

[1] Ulugh Beg Astronomical Institute, Astronomy str. 33, 100052 Tashkent, Uzbekistan
[2] Institute of Fundamental and Applied Research, National Research University TIIAME, Kori Niyoziy 39, 100000 Tashkent, Uzbekistan
[3] Faculty of Computer Engineering, University of Tashkent for Applied Sciences, Gavhar Str. 1, 700127 Tashkent, Uzbekistan
[4] Urgench State University, Kh. Alimjan str. 14, 221100 Urgench, Uzbekistan
[5] Inha University, Ziyolilar 9, 100170 Tashkent, Uzbekistan
[6] School of Science, Harbin Institute of Technology, Shenzhen 518055, China
[7] National Research University TIIAME, Kori Niyoziy 39, 100000 Tashkent, Uzbekistan
[8] Shahrisabz State Pedagogical Institute, Shahrisabz Str. 10, 181301 Shahrisabz, Uzbekistan
[9] Tashkent State Technical University, 100095 Tashkent, Uzbekistan
[10] Institute of Physics, Research Centre for Theoretical Physics and Astrophysics, Silesian University, Bezručovo nám. 13, 74601 Opava, Czech Republic

Received: 28 December 2023 / Accepted: 15 October 2024

Abstract One of the possible ways to test gravity theories and get constraints on parameters of a gravity theory and a black hole is based on studies of black hole shadow applying Event Horizon Telescope (EHT) data from the shadow sizes of M87* and Sgr A*. In this sense, we study the shadow of rotating charged black holes in Einstein–Maxwell scalar (EMS) theory. First, we obtain a rotating EMS black hole solution and analyze the horizon properties. We derive the effective potential for the circular motion of photons along null geodesics around the rotating black hole and obtain the black hole shadow using celestial coordinates. The effects of the black charge and spin and EMS theory parameters on the shape of the black hole shadow, its radius, and distortion parameters are analyzed in detail. We have obtained upper and lower limits for spin and black hole charges of Sgr A* and M87* using their shadow size for various values of EMS parameters. Lastly, we computed and examined the standard shadow radius, equatorial, and polar quasinormal modes using the geometric-optic relationship between the parameters of the quasinormal mode and the conserved values along the geodesics.

1 Introduction

Testing gravity theories, including Einstein's theory of general relativity and modifications or alternatives, is a critical area of theoretical physics and astrophysics research. Various alternative theories to general relativity have been proposed. These include scalar-tensor theories, $f(R)$ gravity, and theories with extra dimensions. These alternatives are tested against observations and experiments.

In the context of the low-energy regime of string theory, it is possible to introduce the dilaton scalar field, which serves as an additional extension to the Einstein action. This extension can take the form of axions, gauge fields, and other complex interactions involving the dilaton and various fields. Researchers have investigated the causal structures and thermodynamic characteristics of black hole solutions that incorporate this dilaton field, as detailed in the specified references [1–10].

An intriguing aspect arises when investigating black hole solutions in the presence of a cosmological constant. The connection between anti-de Sitter solutions and conformal field theory offers a means to unite quantum fields and gravitons. Theories incorporating negative cosmological constants

[a] e-mail: odilbekhamroev@gmail.com
[b] e-mail: javlon@astrin.uz (corresponding author)
[c] e-mail: furqatsariquloff@gmail.com
[d] e-mail: zahid.m0011@gmail.com
[e] e-mail: ahmadjon@astrin.uz
[f] e-mail: zdenek.stuchlik@physics.slu.cz

Published online: 02 December 2024

can be considered integral components of supergravity theories formulated within higher-dimensional spacetime. Several investigations of such gravity theories and black hole solutions are performed in Refs. [11–16].

Within the framework of heterotic string theory, the scalar dilaton field is intricately linked to higher-order expressions involving the electromagnetic field tensor. As a result, when the electromagnetic field tensor is non-zero, it can lead to a non-constant dilaton term. This, in turn, means that in the Reissner–Nordström limit, the solution diverges from being an approximate solution within the context of string theory [2]. In Refs. [17,18], the authors provide estimations of the black hole merger and thin-accretion disc model studied in Einstein–Maxwell-Dilaton theory.

In our previous studies [19–21], we extensively explored the characteristics of the spacetime surrounding charged black holes within the Einstein–Maxwell-scalar (EMS) theory. These investigations involved a comprehensive analysis of the behavior of test particles with electric charge and magnetic dipole moment, shedding light on the structure of the spacetime. Additionally, we also tested EMS gravity through data from astrophysical phenomena, in particular, quasiperiodic oscillations [22]. Recent progress in studying rotating charged black holes within the EMS theory has resulted in important breakthroughs in comprehending their shadow properties. The interplay of charge, rotation, and scalar fields in these black holes significantly influences the form and size of their shadows, providing valuable insights into the gravitational dynamics involved [23]. Studies have shown that scalar fields can cause unique distortions in shadows, making them a valuable tool for evaluating EMS theory using real-world observations [24]. Comparisons with observations from the Event Horizon Telescope (EHT), specifically those of Sgr A* and M87, offer valuable opportunities to refine our understanding of these fascinating objects and constrain theoretical models [25]. By utilizing shadow measurements, we can strengthen our capacity to evaluate predictions of different gravity theories [26]. In addition, examining shadows in alternative theories of gravity, such as scalar-tensor and dilaton-axion models, provides a wider framework for exploring black hole physics [27,28]. These developments highlight the significance of shadow studies in investigating the fundamental aspects of gravity and black hole physics.

In 2019, the EHT Collaboration made a groundbreaking announcement. They unveiled the first image of a black hole, a shadow-like representation of the supermassive black hole located in the center of the M87 galaxy [29]. Their work rendered the black hole physically discernible, enabling them to establish constraints on the size of the black hole's shadow. The revelation of the black hole shadow image in 2019 has significantly heightened scientific interest in investigating black hole shadows. In the context of black hole shadows, one of the initial and notable efforts to quantitatively validate the Kerr metric through shadow analysis was conducted in Refs. [30–32]. Since strong field phenomena are the only indirect tests that can access the event horizon [33], the black hole shadow plays an important role in GR [34]. The shadow is characterized by a central flux depression greater than a factor of approximately 10, along with a compact emission zone with an angular diameter of approximately $\theta_d = 42 \pm 3$ microarcseconds [35–38].

In 2022, researchers from the Event Horizon Telescope (EHT) project presented an image of the black hole at the center of the Milky Way, known as Sgr A*. This image was generated with the assistance of star dynamical priors, which consider the mass and distance estimates derived from the motion of stars in the vicinity of the black hole [39–41], and show that the angular shadow of diameter ($d_{sh} = 48.7 \pm 7$ microarcsecs) According to General Relativity (GR), the recorded images of two black holes, M87* and Sgr A*, are in alignment with the characteristics expected from a Kerr black hole. This consistency suggests that these black holes are well-described by the Kerr metric, which is the solution to the Einstein field equations for a rotating black hole [29,39]. Although Kerr-like black holes arising under modified gravities are not entirely confirmed in the relative deviation of quadrupole moments and the current measurement error of spin or angular momentum, they are not completely excluded [42]. Furthermore, Sgr A * shows concordance with GR predictions of three orders of magnitude in central mass compared to EHT results for M87* [39]. In recent years, studying black hole's shadows has garnered considerable interest, especially considering modified theories of gravity [43–47]. Furthermore, investigating spinning black holes has provided a fresh understanding of these celestial entities' optical characteristics and shadow qualities [48,49]. Furthermore, observational data, such as the data obtained from the EHT, have played a vital role in limiting the range of theoretical parameters [50,51]. Hence, one of the pressing challenges in contemporary astrophysics is the assessment of modified or alternative gravity models using the data provided by the EHT Collaboration.

In Ref. [52], the shadow of the Simpson–Visser black holes (wormholes) was recently investigated. Constraints on the length parameter were obtained using the image size of supermassive black holes/wormhole candidates at the center of galaxies M87 and Milky Way observed by EHT observations. The similarity of the SV black hole shadow and the shadow of the Kerr black holes was given. However, the SV wormhole (with $l > 2$) with a large spin can cast a closed photon ring. Gravitational lensing and retrolensing in both weak and strong gravitational field limits, together with quasinormal spectra and gray-body factors, have been studied in Refs. [53–56]. Also, the strong deflection limits of the Simpson–Visser spacetime have been studied in Refs. [57,58] and found that the photonsphere around the

SV spacetime does not depend on (weakly depend on) the length parameters when $l \leq 3$. This implies that distinguishing the black hole from the wormhole in the SV metric is not possible.

Furthermore, the investigation of the interaction between the electric charge of Schwarzschild-de Sitter black holes and the parameters governing the bounce effect was carried out in the study referenced as [59]. This study revealed that the orbital motion around black-bounce-Reissner–Nordström black holes closely resembles that around Schwarzschild black holes, thus highlighting the degeneracy in their effects.

To mitigate the degeneracy properties of the black hole parameters, the relationship between black hole charge and bounce parameters has been explored to utilize precession data obtained from the S2 star orbits around Sgr A* as detected by the GRAVITY Collaboration. Additionally, measurements of the shadow size of Sgr A* by the Event Horizon Telescope (EHT) have been employed. Similar tests involving various black holes within different gravity theories and utilizing observations from both the EHT and GRAVITY Collaborations have been conducted as outlined in Refs. [60–66].

The main focus of this paper is to explore the behavior of photon motion in the vicinity of charged rotating black holes within the framework of EMS theory. We also focus on understanding the optical properties of the spacetime around the black hole, including the presence of a photon sphere, an appearance, and distortion of the black hole's shadow. Furthermore, we derived constraints on the charge of the black holes and the parameters of EMS theory using data from the Event Horizon Telescope (EHT), particularly the shadow sizes of the supermassive black holes SgrA* and M87*. Additionally, we analyzed the emission rate of rotating EMS black hole evaporation through Hawking radiation near the black hole horizon.

The work is organized as follows: in Sect. 2, we provide a brief explanation of charged black hole solutions in EMS theory and obtain a rotating charged black hole solution using the NJA. Also, we study the horizon properties of the obtained rotating black hole spacetime. The null geodesic equations are derived in the spacetime of the rotating black hole, and circular photon orbits around the rotating black holes are investigated in Sect. 3. Also, we studied the radius and deviation parameters of the shadow of the black hole in Sect. 3. Section 4 is devoted to getting constraint values on the black hole charge and spin parameters for different values of the EMS parameters using data from the image sizes of Sgr A* and M87* measured by EHT Collaboration. Finally, we discuss and summarize our main results in Sect. 6.

2 Charged rotating EMS black holes

In this section, we intend to present the black hole solution of the EMS field equations. The action that governs the gravitational field of the EMS theory is given as [1,2,67],

$$S = \int d^4x\sqrt{-g}\Big[R - 2\nabla_\alpha\phi\nabla^\alpha\phi - K(\phi)F_{\alpha\beta}F^{\alpha\beta} - V(\phi)\Big], \tag{1}$$

where ∇_α represents the covariant derivative, g denotes the determinant of the metric tensor $g_{\mu\nu}$, R corresponds to the Ricci scalar characterizing curvature, and ϕ is the massless scalar field, $F_{\alpha\beta}$ represents the electromagnetic field tensor, and $K(\phi)$ denotes the coupling function between the dilaton field and the electromagnetic fields, and finally, $V(\phi)$ stands for the potential of the scalar field.

By applying the principle of least action and varying the action (1) for the metric $g_{\alpha\beta}$, the vector potential A_α, and the dilaton (scalar) ϕ fields, we derive the equations of motion for the EMS system in the following form [67]

$$R_{\alpha\beta} = 2\nabla_\alpha\phi\nabla_\beta\phi + \frac{1}{2}g_{\alpha\beta}V + 2K\left(F_{\alpha\gamma}F_\beta{}^\gamma - \frac{1}{4}g_{\alpha\beta}F_{\mu\nu}F^{\mu\nu}\right), \tag{2}$$

$$\nabla_\alpha\left(KF^{\alpha\beta}\right) = 0, \tag{3}$$

$$\nabla_\alpha\nabla^\alpha\phi - \frac{1}{4}\left(V_{,\phi} + K_{,\phi}F_{\mu\nu}F^{\mu\nu}\right) = 0, \tag{4}$$

where $_{,\phi}$ denotes derivative with respect to the dilaton field, $R_{\alpha\beta}$ is the Ricci tensor.

It's evident that Eqs. (2)–(4) represent a system of coupled differential equations, making it challenging to discover exact solutions for such a system of nonlinear equations. However, it is possible to find exact analytical solutions for complex systems under certain assumptions.

In Ref. [67], the authors obtain the exact analytical solutions for spacetime around the static spherically symmetric black hole in EMS theory in the following general form:

$$ds^2 = -f(r)dt^2 + \frac{dr^2}{f(r)} + h(r)(d\theta^2 + \sin^2\theta d\phi^2), \tag{5}$$

where $f(r)$ and $h(r)$ are radial functions. In Ref. [67] Authors have used the following special form for the function $K(\phi)$

$$K(\phi) = \frac{2e^{2\phi}}{\beta e^{4\phi} + \beta - 2\gamma} \tag{6}$$

and obtained the solution in the form

$$f(r) = 1 - \frac{2M}{r} + \frac{\beta Q^2}{h(r)}$$

$$h(r) = r^2\left(1 + \frac{\gamma Q^2}{Mr}\right). \tag{7}$$

Spacetime metric (5) with the functions (7) is the solution of static and spherically symmetric black holes in EMS theory. When the conditions $\beta = 1$ and $\gamma = 0$ are applied, the Reissner–Nordström solution can be obtained, and the metric reduces to Schwarzschild black hole at $\beta = \gamma = 0$.

The metric of a rotating black hole is considered one of the most straightforward extensions of a static black hole, incorporating an extra spin component conventionally represented by the symbol a. The characteristics and dynamics of the spacetime framework surrounding a revolving black hole exhibit notable distinctions compared to its static counterpart, particularly regarding the trajectory of photons. Estimating the significance of a revolving black hole can be achieved using an analysis that compares the black hole's shadow with the observational data obtained from the EHT for supermassive black holes. Given that supermassive black holes exhibit rotation, it is advisable to consider rotating black holes for a comprehensive and precise analysis of their shadows.

The Newmann–Janis Algorithm (NJA) was developed to construct rotating solutions for black hole metrics within the framework of general relativity (GR) [68,69]. Black holes commonly possess only three fundamental parameters: mass, spin, and charge. In a study conducted by Hansen and Yunes in 2013, it was discovered that applying the No-Hair Theorem to static black holes within gravity theories other than general relativity reveals the emergence of hitherto unidentified characteristics of black holes. In recent research undertaken by Azreg-Aïnou, improvements were made to the NJA to obtain rotating counterparts without encountering additional challenges [70,71]. Therefore, this approach can be readily implemented for black hole metrics in general relativity and modified gravity theories.

In recent works, the rotating black hole metrics have been successfully constructed from non-rotating black hole solutions [72,73]. Hence, we employ the modified NJA method to derive the rotational version of the static metric (5). Initially, we introduce the Eddington-Finkelstein coordinates (u, r, θ, ϕ) and proceed by employing the corresponding transformation

$$du = dt - \frac{dr}{f(r)}, \tag{8}$$

the static metric (5) is transformed to the form

$$ds^2 = -f(r)du^2 - 2dudr + r^2d\theta^2 + r^2\sin^2\theta d\phi^2. \tag{9}$$

Moreover, the conjugate metric tensor can be represented as follows:

$$g^{ab} = -l^a n^b - n^a l^b + m^a\bar{m}^b + \bar{m}^a m^b, \tag{10}$$

where the null tetrads are defined as:

$$l^a = \delta^a_r, \tag{11}$$

$$n^a = \delta^a_u - \frac{f(r)}{2}\delta^a_r, \tag{12}$$

$$m^a = \frac{1}{\sqrt{2}r}\left(\delta^a_\theta + \frac{i}{\sin\theta}\delta^a_\phi\right). \tag{13}$$

The symbol $\bar{m}^a$ represents the complex conjugate of m^a. It is readily apparent that the aforementioned null tetrads exhibit the following relationships:

$$l_a l^a = n_a n^a = m_a m^a = \bar{m}_a\bar{m}^a = 0, \tag{14}$$

$$l_a m^a = l_a\bar{m}^a = n_a m^a = n_a\bar{m}^a = 0, \tag{15}$$

$$-l_a n^a = -l^a n_a = m_a\bar{m}^a = m^a\bar{m}_a = 1. \tag{16}$$

In this analysis, we proceed with the intricate coordinate transformations within the (u, r)-plane,

$$u' \to u - ia\cos\theta, \quad r' \to r + ia\cos\theta, \tag{17}$$

where a is the spin parameter of the black hole.

The subsequent NJA stage introduces complexity to the radial coordinate, denoted as r. However, it is not deemed essential, as demonstrated by the findings in the study conducted by [70]. The compactification process can be avoided by considering the transformation properties of δ^μ_ν as a vector under transformation (17). Simultaneously, the metric functions associated with the metric (9) transform unspecified functions

$$f(r) \to F(r, a, \theta), \quad r^2 \to H(r, a, \theta), \tag{18}$$

in such a manner

$$\lim_{a\to 0} F(r, a, \theta) = f(r), \quad \lim_{a\to 0} H(r, a, \theta) = r^2. \tag{19}$$

Through these changes, the null tetrads are altered

$$l^a = \delta^a_r, \tag{20}$$

$$n^a = \delta^a_u - \frac{F}{2}\delta^a_r, \tag{21}$$

$$m^a = \frac{1}{\sqrt{2H}}\left((\delta^a_u - \delta^a_r)ia\sin\theta + \delta^a_\theta + \frac{i}{\sin\theta}\delta^a_\phi\right). \tag{22}$$

Utilizing the new null tetrads, the rotating metric in the Eddington-Finkelstein coordinates is as follows:

$$\begin{aligned} ds^2 = &-Fdu^2 - 2dudr + 2a\sin^2\theta(F-1)dud\phi \\ &+2a\sin^2\theta drd\phi + Hd\theta^2 \\ &+\sin^2\theta\left(H + a^2\sin^2\theta(2-F)\right)d\phi^2. \end{aligned} \tag{23}$$

By transforming these coordinates to the Boyer-Lindquist coordinates, we may get the rotational counterpart for the static black hole metric (5). Hence, the implementation of global coordinate transformations is proposed

$$du = dt + \lambda(r)dr, \tag{24}$$

$$d\phi = d\phi' + \chi(r)dr, \tag{25}$$

with

$$\lambda(r) = -\frac{a^2 + r^2}{a^2 + r^2 f(r)}, \tag{26}$$

$$\chi(r) = -\frac{a}{a^2 + r^2 f(r)}. \tag{27}$$

Furthermore, it is possible to compose as follows:

$$F = \frac{\left(r^2 f(r) + a^2 \cos^2\theta\right)}{H}, \tag{28}$$

$$H = r^2 + a^2 \cos^2\theta. \tag{29}$$

Then, the rotational version of the black hole metric in the context of Einstein–Maxwell scalar theory is described as follows.

$$\begin{aligned} ds^2 = &-\frac{\Delta - a^2 \sin^2\theta}{\Sigma} dt^2 + \frac{\Sigma}{\Delta} dr^2 + \Sigma d\theta^2 \\ &+ \frac{(\Sigma + a^2 \sin^2\theta)^2 - a^2 \sin^2\theta \Delta}{\Sigma} \sin^2\theta d\phi^2 \\ &- 2\frac{a\left(2Mr + (2\gamma - \beta)Q^2\right)}{\Sigma} \sin^2\theta d\phi dt \end{aligned} \tag{30}$$

where

$$\Sigma = r^2 + a^2 \cos^2\theta + \frac{\gamma Q^2}{Mr}, \tag{31}$$

$$\Delta = r^2 + a^2 - 2Mr + Q^2\left[\beta + \gamma\left(2 - \frac{r}{M}\right)\right]. \tag{32}$$

It is evident that as the limit $a \to 0$ is approached, the metric (30) undergoes a reduction to the static metric (5) while simultaneously satisfying the conditions (19). When conditions $\gamma = 0$ and $\beta = 1$ are applied to the metric (30), it results in the Kerr–Newman black hole solution, which is further simplified to the Kerr black hole when the charge vanishes ($Q = 0$).

To investigate the structure of the event horizon of the rotating black hole in EMS theory, as described by the metric (30), we proceed by solving the equation $g^{rr} = 0$ to obtain the roots that correspond to the radius of the horizon.

In Fig. 1, we presented an analysis of the relationship between the radius of the horizon and the parameters of an EMS black hole. On the left panel, black and red dashed legends correspond to the Kerr and Kerr–Newman black holes, respectively, according to the chosen fixed values of parameters. Therefore, following this graph when comparing rotating black holes in Einstein–Maxwell-Scalar (EMS) theory and the Kerr and Kerr–Newman solutions makes sense. What can be revealed from Fig. 1 is that an increase in the value of parameter β, at $\gamma = 0$, causes an extreme value of charge Q increase. In contrast, the limiting value of Q decreases with an increase of β when γ is less than zero. Furthermore, there are apparent differences in the positive and negative values of the parameter, γ, as described in the right panel.

The behavior of the horizon of the black hole by varying parameters is illustrated in Fig. 2. We can see from these pictures that some values of the parameters of the black hole may have one horizon. For instance, if we fix $\gamma = 0$ and $\beta = 0.5$, there is one horizon in $a/M = 0.8$ and $Q/M = 0.85$. A further increase in Q/M causes the black hole's horizon to disappear. To these properties, we can construct some expression for the maximum spin that separates with black hole and naked singularity. From the set of conditions, $\Delta = 0 = \Delta'$ we can easily find,

$$a_{max} = \frac{M}{2}\sqrt{\left(2 + \gamma\frac{Q^2}{M^2}\right)^2 - 4\frac{Q^2}{M^2}\beta}\ , \tag{33}$$

where the prime denotes the derivative with respect to r. From this, we find the highest value of a appears when $\beta = 0$ and $\gamma = 0$ cases write as follows,

$$\frac{a_{max}}{M} = 1 + \frac{\gamma Q^2}{2M}, \quad \text{and,} \quad \frac{a_{max}}{M} = \sqrt{1 - \beta\frac{Q^2}{M^2}}\ , \tag{34}$$

respectively. It is easy to see that this value is more than one for $\gamma > 0$ and less than one for $\gamma < 0$.

It is well-known that the selection of black hole parameters is subject to certain limits, and it is impossible to choose values for these parameters arbitrarily. Whether an object is a black hole or a naked singularity depends on the presence or absence of an event horizon. In Fig. 3, we described the black hole region depending on the values of the black hole parameters. One can conclude that an increase in the β parameter leads to a decrease in the maximum spin, and a decrease in γ increases the range of maximum spin and charge values.

3 Null geodesics and the black hole shadow

We start this section by examining the geodesic structure surrounding the rotating black hole in the EMS theory, as described by Eq. (30). We will analyze the circular photon orbits around a black hole by considering the effective potential, a crucial parameter for investigating the shadow produced by a rotating black hole. Geodesic equations must be solved to determine the motion of the particles in a given background. The derivation of geodesic equations can be accomplished using the Hamilton–Jacobi (HJ) method. The HJ equation that characterizes the motion of a particle is given by

$$\frac{\partial S}{\partial \tau} = -\frac{1}{2} g^{\mu\nu} \frac{\partial S}{\partial x^\mu} \frac{\partial S}{\partial x^\nu}, \tag{35}$$

where τ is the affine parameter. In the context of the black hole metric being examined, there are two Killing vector

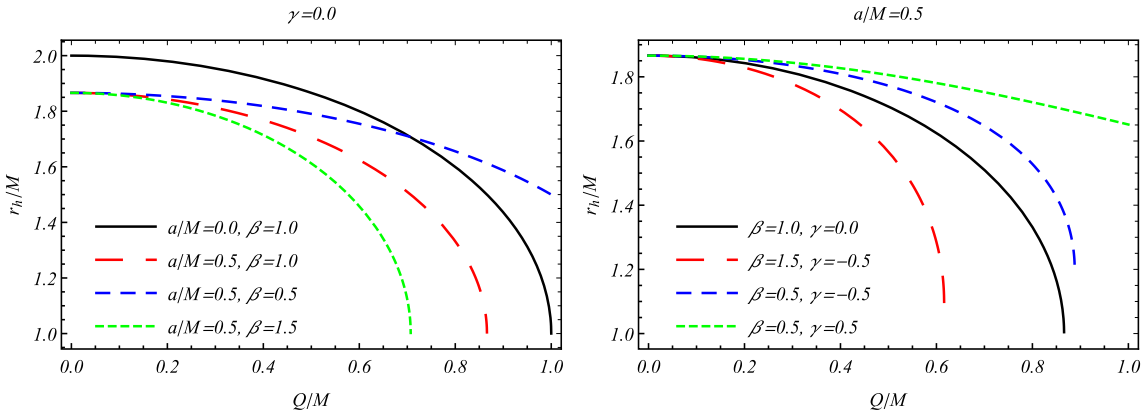

Fig. 1 Dependence of the event horizon radius of the black hole with parameters a, β, γ and Q

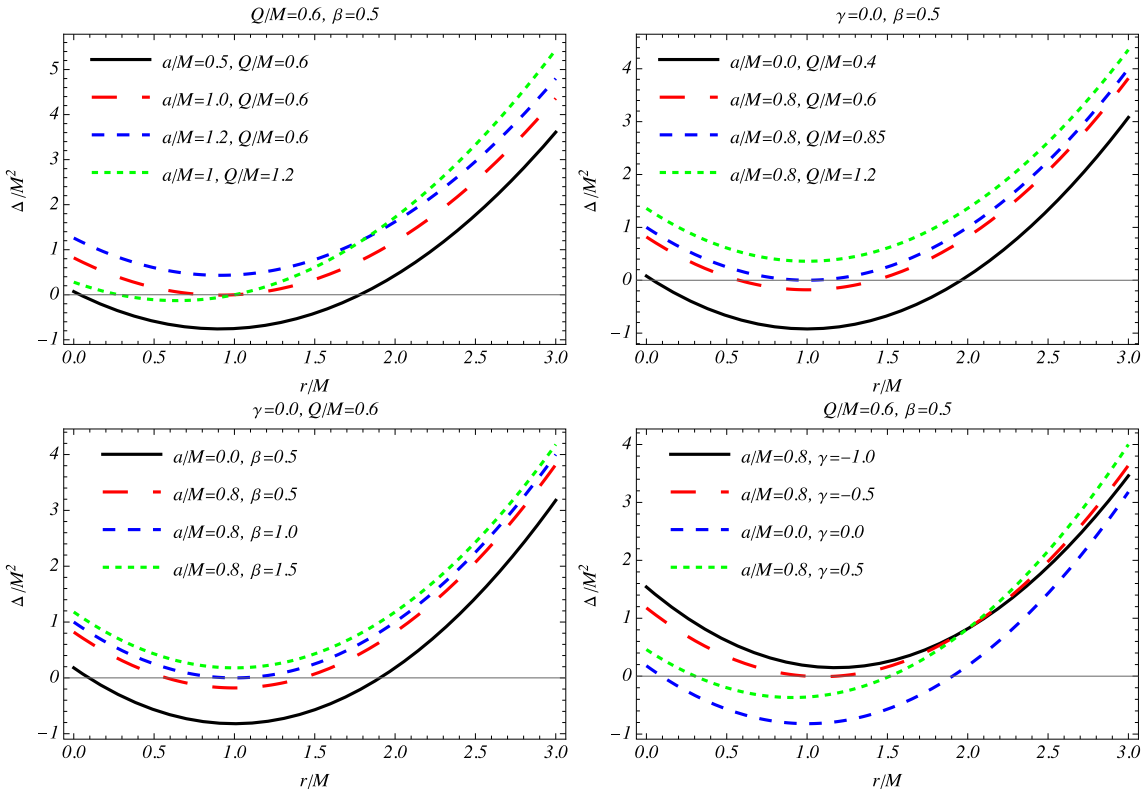

Fig. 2 Dependency between Δ and r in different value of parameters a, Q, β and γ

fields denoted as ∂_t and ∂_ϕ, representing translational and rotational invariance with respect to proper time. These vector fields give rise to two constants of motion, namely the particle energy E and the orbital angular momentum L,

$$-E = g_{t\mu}\dot{x}^\mu = p_t, \tag{36}$$

$$L = g_{\phi\mu}\dot{x}^\mu = p_\phi, \tag{37}$$

The variables p_t and p_ϕ represent the generalized momenta in their respective orientations. It can be postulated that the Jacobi action can be expressed in the following way,

$$S = \frac{1}{2}m_p^2\tau - Et + L\phi + S_r(r) + S_\theta(\theta). \tag{38}$$

The symbol m_p represents the rest mass of the particle. The functions $S_r(r)$ and $S_\theta(\theta)$ are dependent solely on the variables r and θ, and their specific forms are still undetermined. By substituting the Jacobi action (Eq. 38) into the Hamilton–Jacobi equation (Eq. 35) and taking into account that a photon

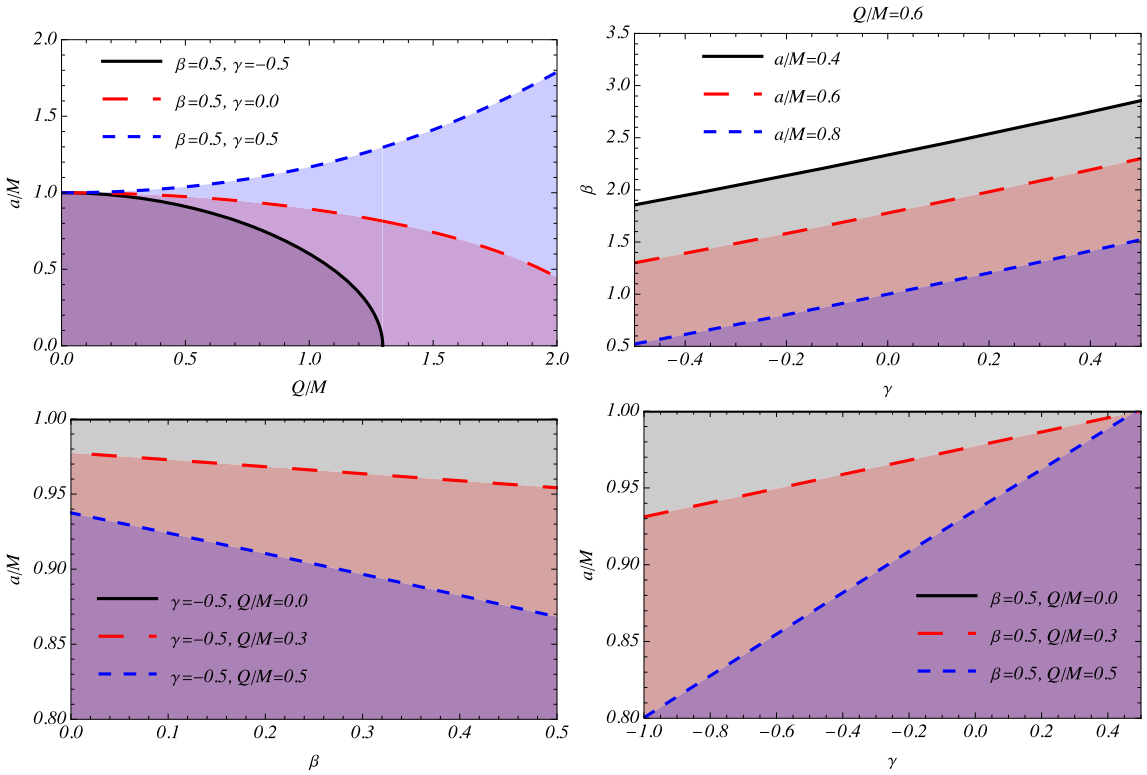

Fig. 3 Relationship between the extremal black hole parameters

mass is zero, one may get the following expressions

$$S_r(r) = \int^r \frac{\sqrt{\mathcal{R}(r)}}{\Delta(r)} dr, \quad S_\theta(\theta) = \int^\theta \sqrt{\Theta(\theta)} d\theta, \tag{39}$$

with

$$\mathcal{R}(r) = \Big[E(h(r) + a^2) - aL\Big]^2 - \Delta(K + (L - aE)^2), \tag{40}$$

$$\Theta(\theta) = K + \cos^2\theta \left(a^2E^2 - \frac{L^2}{\sin^2\theta}\right), \tag{41}$$

Here, the symbol K represents the Carter constant, associated with the Killing–Yano tensor field, and serves as the fourth constant of the geodesics. Given that there are four equations associated with four coordinate variables and the system of equations is fully integrable, it follows that there are four constants. In the case of the photon motion, we have restricted the mass as $m_p = 0$. By computing the derivatives of the Hamilton–Jacobi action for the four constants as mentioned above and, after that, solving the resulting equations by equating them to zero, we can derive the subsequent geodesic equations,

$$\Sigma \frac{dt}{d\tau} = a(L - aE\sin^2\theta) + \frac{h + a^2}{\Delta}(E(h + a^2) - aL), \tag{42}$$

$$\Sigma \frac{dr}{d\tau} = \pm\sqrt{\mathcal{R}}, \tag{43}$$

$$\Sigma \frac{d\theta}{d\tau} = \pm\sqrt{\Theta}, \tag{44}$$

$$\Sigma \frac{d\phi}{d\tau} = \left(\frac{L}{\sin^2\theta} - aE\right) + \frac{a}{\Delta}(E(h + a^2) - aL). \tag{45}$$

The present investigation centers on examining circular photon orbit by analyzing radial motion. The significance of the circular motion of photons is crucial in this investigation. The equation denoted as (43) can alternatively be formulated as the radial geodesic equation,

$$\frac{1}{2}\left(\Sigma \frac{dr}{d\tau}\right)^2 + V_{eff} = 0, \tag{46}$$

where V_{eff} is the effective potential. It takes the following form in the equatorial plane,

$$V_{eff} = -\frac{\mathcal{R}(r)}{2r^4}. \tag{47}$$

The following standard conditions give the unstable circular photon orbits forming the Black hole shadow,

$$V_{eff} = 0, \quad \frac{\partial V_{eff}}{\partial r} = 0, \quad \frac{\partial^2 V_{eff}}{\partial r^2} < 0. \tag{48}$$

Introducing the new definitions $\xi = \frac{L}{E}$ and $\eta = \frac{K}{E^2}$, and solving the equations in (48), the following results are obtained

[74]

$$\xi = \frac{\left(a^2+h\right)\Delta' - 2\Delta h'}{a\Delta'}, \tag{49}$$

$$\eta = \frac{4a^2\Delta h'^2 - \left(\Delta' h - 2\Delta h'\right)^2}{a^2\Delta'^2}. \tag{50}$$

3.1 Black hole shadow

We are interested in investigating the shadow produced by the rotating black hole within the framework of the EMS theory. It is useful to mention that, in our particular scenario, all light sources are positioned at an infinite distance and are uniformly scattered in all directions. Furthermore, it is important to note that there is no discernible light source between the black hole and the observer. We assume that the observer is at an infinite distance from the black hole. The shadow images, based on the assumptions stated above, are determined by two celestial coordinates [75]

$$\begin{aligned}\mu &= -\lim_{r_0\to\infty}\left(r_0^2\sin\theta_0\frac{d\phi}{dr}\bigg|_{\theta\to\theta_0, r\to r_0}\right)\\ &= -\xi(r_p)\csc\theta_0,\end{aligned} \tag{51}$$

$$\begin{aligned}\lambda &= \lim_{r_0\to\infty}\left(r_0^2\frac{d\theta}{dr}\bigg|_{\theta\to\theta_0, r\to r_0}\right)\\ &= \pm\sqrt{\eta(r_p)+a^2\cos^2\theta_0-\xi(r_p)^2\cot^2\theta_0}.\end{aligned} \tag{52}$$

The variable θ_0 represents the inclination angle of the observer relative to the symmetry axis of the spacetime. When the viewer is situated on the equatorial plane, the celestial coordinates are rendered in a simpler form

$$\mu = -\xi(r_p), \quad \lambda = \pm\sqrt{\eta(r_p)}. \tag{53}$$

The shadow can be acquired by generating a parametric representation in the celestial plane of μ-λ, which adheres to the Eqs. (49) and (50). The parameter that governs the representation is denoted as r_p. As mentioned above, the zone does not get illumination from sources that emit photons. Determining the shadow's boundary is contingent upon the radius of the circular photon orbits.

In Fig. 4, the shadow images of rotating black holes in EMS theory have been illustrated in different ranges of the parameters a, Q, β, and γ. These plots explain how the size of the shadow changes depending on black hole parameters. The size of the shadow region diminishes as the Q parameter increases, and the shape of the shadow becomes more distorted as the Q/M approach's unity. Moreover, the shadow area experiences a reduction as the parameter β increases, whereas the shadow radius increases with increasing value of γ.

3.2 Shadow observables

The silhouette of the black hole serves as a distinctive representation of the characteristics of the surrounding spacetime in terms of its configuration and dimensions. Therefore, this approach can be a valuable technique for evaluating novel theories of gravity and limiting the parameters associated with black holes. Constraints for the black hole parameters can be obtained by utilizing shadow observables. It is necessary to establish the measurable variables that delineate the shape and size of the black hole's silhouette to accomplish this. For the first time, Hioki and Maedia developed two observational parameters related to the black hole shadow [76]; for an alternative approach, see Ref. [77]. The first parameter, known as the shadow radius, quantifies the shadow's size. The second parameter is called the deviation parameter, which is used to characterize the distortion exhibited by the circular shape of the shadow.

The characteristic of being circular is exclusive to static black holes, whereas rotating black holes possess a different set of characteristics. Hence, an investigation of distortion is conducted to analyze the contrast between shadows of rotating black holes and static black holes and those exhibiting minimal distortion in their shadows. A readily observable parameter quantifies the measurement of distortion called the linear radius of the shadow, as determined in previous studies [76,78].

$$R_{sh} = \frac{(\mu_t-\mu_r)^2+\lambda_t^2}{2|\mu_t-\mu_r|}, \tag{54}$$

The variable R_{sh} represents the radius of a theoretical circle that is expected to contact the shadow curve at three specific places: (μ_t, λ_t), (μ_b, λ_b), and $(\mu_r, 0)$. The shadow of the black hole can be defined as the set of points in the space (μ, λ), where each point is identified by the subscripts t, b, and r, denoting the top, bottom, and rightmost points, respectively. Please consult Figure 9 in Ref. [78] for additional information. Equation (54) is relevant exclusively to rotating black holes, as static black holes possess circular shadows that the coordinates of the curve may describe on any coordinate axes. Subsequently, the distortion can be acquired through the established equation.

$$\delta_s = \frac{|\bar{\mu}_l - \mu_l|}{R_{sh}}. \tag{55}$$

The points $(\mu_l, 0)$ and $(\bar{\mu}_l, 0)$ overlap the $-\mu$ axis, the former residing in the shadow and the latter in the imaginary circle. The points on the shadow are identified by the subscript l positioned on the left side of the λ-axis. In contrast, the locations on the imaginary circle are indicated by the presence of a bar.

Figure 5 illustrates the graphical representation of the variation in distortion with the spin parameters of the black

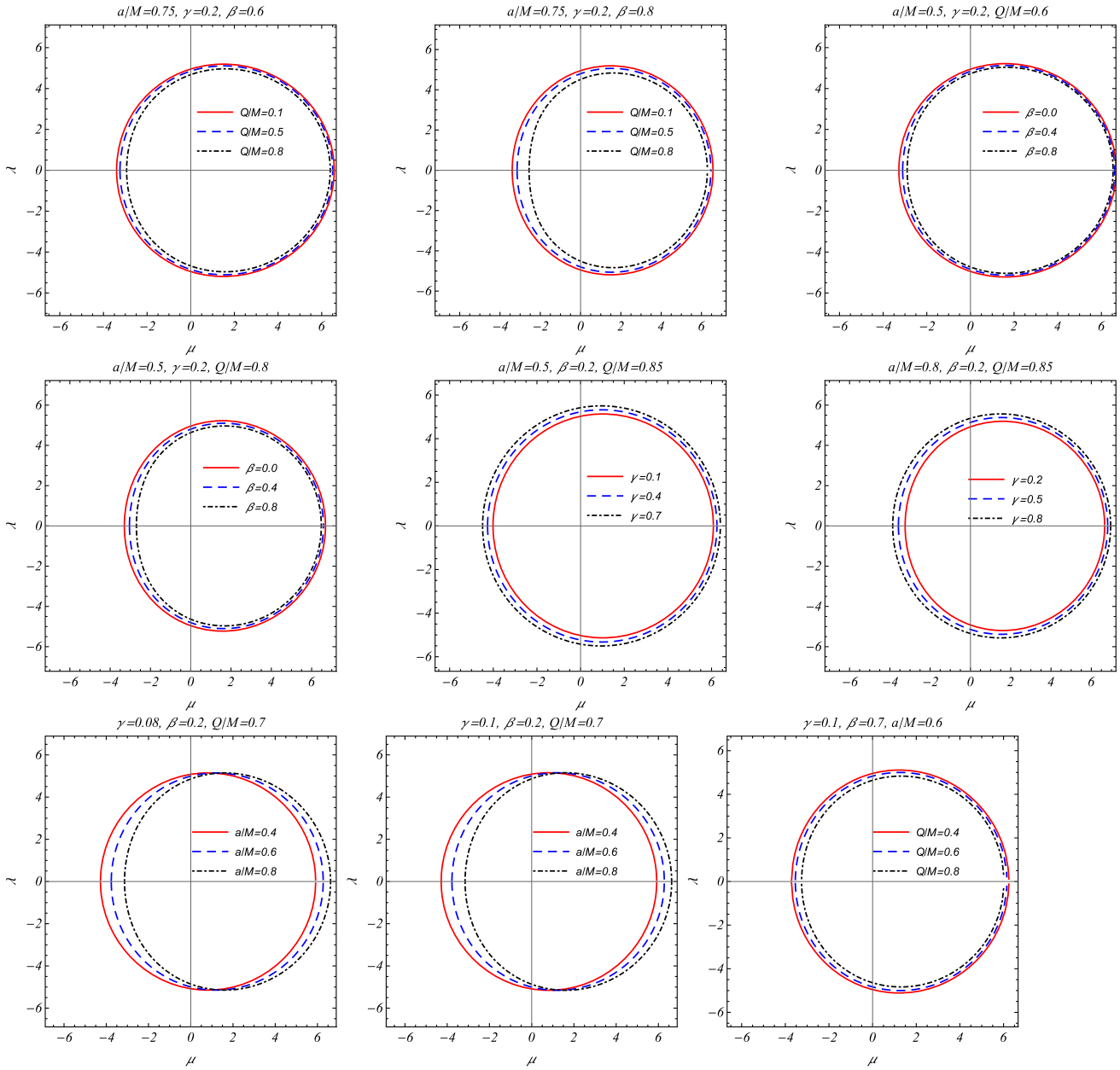

Fig. 4 Black hole shadow for various parameter a, γ, Q and β

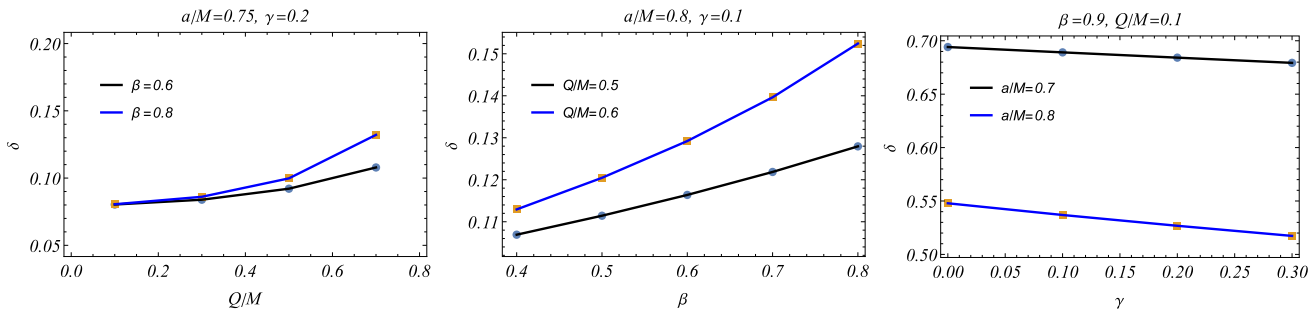

Fig. 5 Variation of the δ with respect to charge parameter Q (upper left panel), β (upper right panel), parameter γ (lower left panel) and spin parameter a (lower right panel)

hole a, charge Q, and the parameters of the EMS theory, β and γ. The distortion parameter increases sufficiently with increased black hole spin and charge values. However, the effects of the parameters of the scalar field γ and β on δ become stronger at higher values of Q and a. The top left panel shows that the difference of δ in the cases $\beta = 0.6$ and $\beta = 0.8$ is negligible when $Q \leq 0.5M$ or less than the error in measurements of shadow distortion.

In addition to the approach proposed by Hioki and Maeda, an alternative method can be utilized to estimate the black hole parameter. This method is based on the coordinate independent formalism [79,80] and leverages the shadow observables, namely the shadow area and oblateness. The concepts of the black hole shadow area denoted as A, and oblateness, denoted as D, can be introduced as [80,81]

$$A = 2\int_{r_-}^{r_+} \lambda(r)\frac{d\mu(r)}{dr}dr, \tag{56}$$

$$D = \frac{\Delta\mu}{\Delta\lambda}, \tag{57}$$

where $r_\pm$ are radii of stable circular photon orbits obtained by solving the equation $\eta_c = 0$ [82].

The dependencies of the shadow area A and the oblateness D on the parameters of a rotating black hole in EMS theory are plotted in Figs. 6 and 7. These dependencies are obtained using numerical computations. What can be revealed from Fig. 6 is that the observable parameter A decreases with an increase of a and Q, while the shadow area increases when γ increases. Similarly, oblateness D also decreases with an increase in spin and charge parameters and increases within the influence of the parameter γ. In addition, the parameter β causes a decrease in the values of both area and oblateness.

4 Comparison with EHT data

The acquisition of observational data on the shadow images of two supermassive black holes, namely Sgr A* and M87*, through the collaborative efforts of the Event Horizon Telescope (EHT), serves as a compelling impetus for the scientific community to undertake further investigations into the study of black hole shadows. Using the provided data, it is possible to constrain the black hole parameters within the context of several modified or alternative gravity models [81,83–89]. This allows for an evaluation of whether the outcomes of the model align effectively with theoretical proposals. In our study, we incorporate constraints on the parameters of the rotational black hole in the EMS theory based on the observational outcomes obtained from the Event Horizon Telescope (EHT) observations of M87* and Sgr A*.

The restrictions were obtained by utilizing the angular diameters of the two black holes, as estimated by the EHT team. The angular diameter of the shadow picture observed by an observer located at a distance d from the black hole can be mathematically represented as

$$\theta_d = 2\frac{R_a}{d}, \quad R_a = \sqrt{\frac{A}{\pi}} \tag{58}$$

where R_a is the area shadow radius. When Eq. (56) is taken into account, it can be observed that the angular diameter of the shadow is contingent upon the properties of the black hole and the observation angle. Additionally, the dependence on the mass of the black hole is implicit.

Now, we examine the rotating black holes M87* and Sgr A* within the context of the EMS theory. Our objective is to compare the theoretical results of shadow analysis with the shadow images obtained from observational data of M87* and Sgr A* captured by the Event Horizon Telescope. The mass of the supermassive black hole known as M87* and its distance from Earth are denoted as $M = 6.5 \times 10^9 M_\odot$ and $d = 16.8Mpc$, respectively, as reported in references [37,38]. To maintain simplicity, we have disregarded the uncertainties associated with the observations of mass and distance of supermassive black holes. According to the findings of the Event Horizon Telescope [29], the angular diameter of the picture of the supermassive black hole M87* is measured to be $\theta_d = 42 \pm 3\mu as$ at a 1-σ confidence level.

In Fig. 8, we show the density visualizations of the angular diameter θ_d in the a-Q domain for the various fixed values of β and γ. The black curves represent the lower boundaries of the measured angular diameter of the black hole M87* shadow image. It can be seen that when we choose the positive parameter γ instead of the negative one, the threshold value of Q/M is almost double (approximately 0.35 to 0.76): in addition, reducing the parameter β leads to a decrease in the restricted area.

Constraints on the shadow image of Sgr A* can also be derived from the EHT data. The angular diameter of the shadow of the supermassive black hole Sgr A* is measured to be $\theta_d = 48.7 \pm 7\mu as$ according to the Event Horizon Telescope [39]. The mass of Sgr A* and its distance from the solar system are estimated to be approximately $4 \times 10^6 M_\odot$ and 8 kpc, respectively [40,41].

The limitations of Sgr A * are described in Fig. 9 for the two scenarios for inclination angles of 90° and 50°. The black curves correspond to the mean value of the measured angular diameter of Sgr A*. In the lower panels, the density plots obtained from fitting the data show that the black hole angular diameter is within the range of the reported angular diameter of Sgr A*, which is $\theta_d = 48.7 \pm 7\mu$as. Hence, we may assert that our theoretical findings about the rotating EMS black hole can theoretically match the supermassive black hole at our galaxy's core. The figure indicates an increase in the upper limit of the charge parameter Q (which rises from around $0.58M$ to over $0.7M$) as the fixed value of the parameter β decreases. However, there is a significant

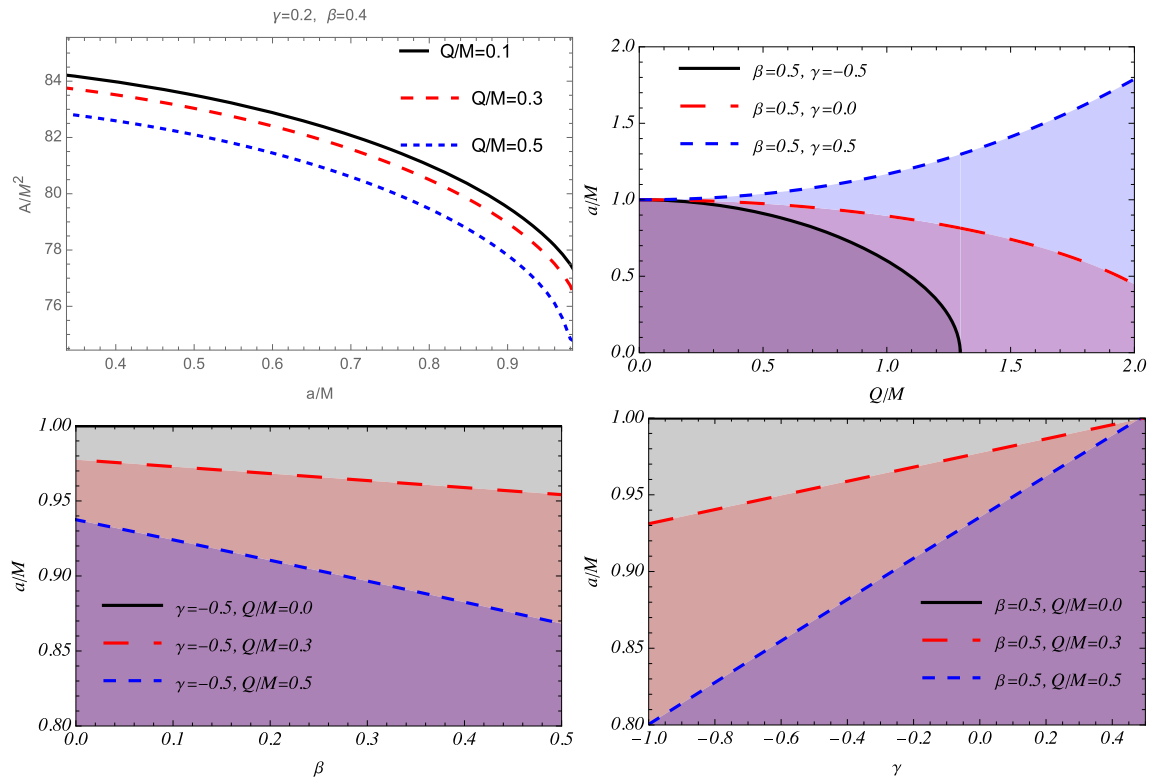

Fig. 6 Variation of the shadow area with respect to spin parameter a (left panel) and charge Q (right panel)

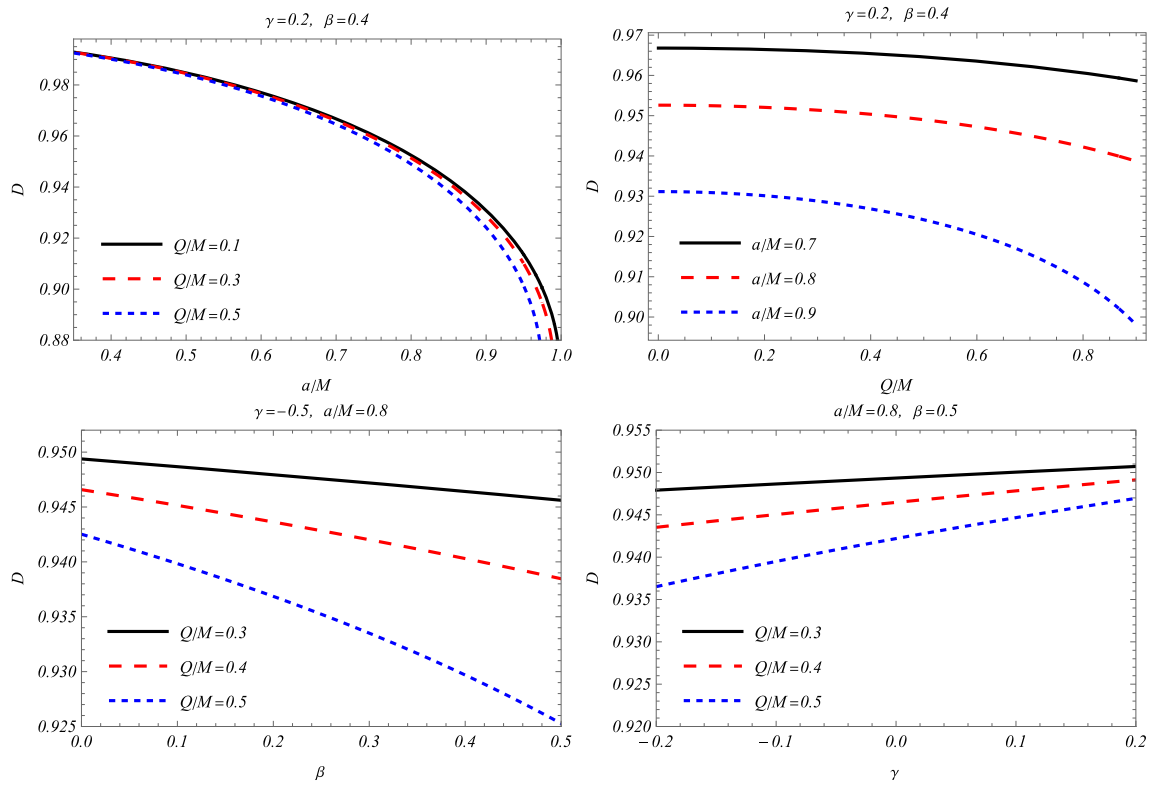

Fig. 7 Variation of the oblateness with respect to spin parameter a (left panel) and charge Q (right panel)

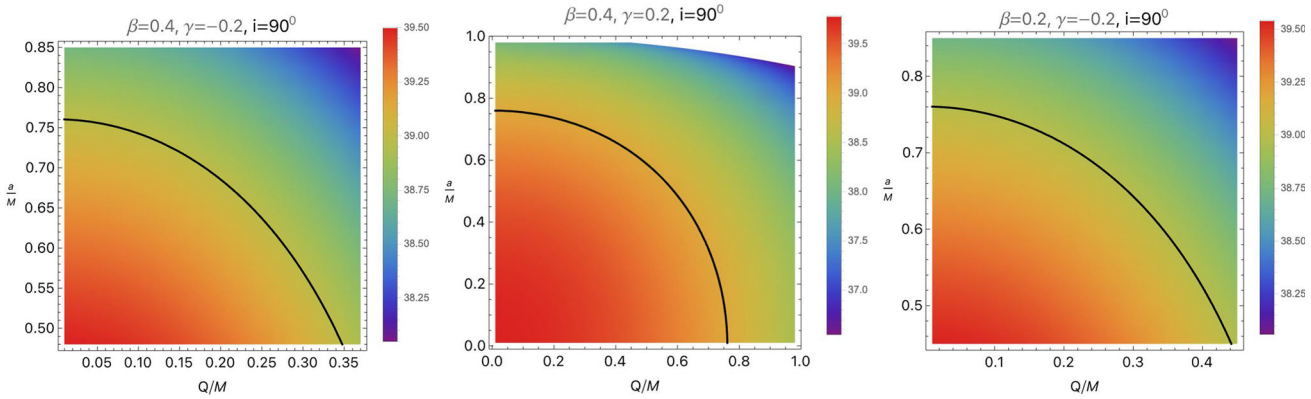

Fig. 8 Variation of the angular diameter observable for spin parameter a and charge Q with fixed parameters $\gamma = 0.2$ and $\beta = 0.4$ (left panel) and parameter β with fixed parameters $Q/M = 0.3$ and $\gamma = 0.2$ (right panel) for $M87^*$. The bar chart represents the angular diameter

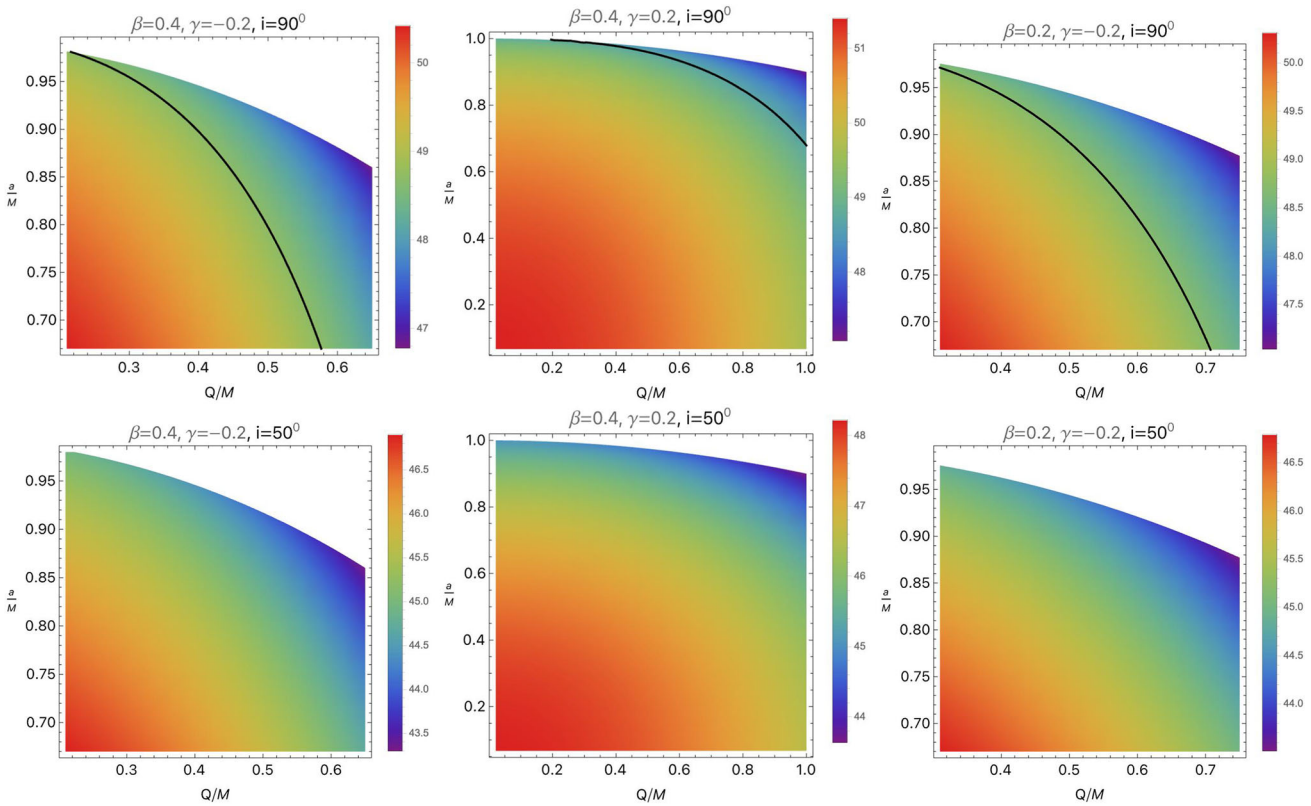

Fig. 9 Variation of the angular diameter observable for spin parameter a and charge Q with fixed parameters $\gamma = 0.2$ and $\beta = 0.4$ for inclination angle 90^0(left panel) and 50^0 (right panel) for Sgr. A^*. The bar chart represents the angular diameter

disparity between the instances when the parameter γ has contrasting values. Furthermore, an alteration of the inclination angle impacts the angular diameter variation in the a-Q space. These density plots allow for examining the relationship between the angular diameter of the black hole shadow and its parameters. Therefore, this study clearly shows that one can estimate black hole parameters using observational data of black hole shadows.

5 Equatorial and polar QNMs and their relation with typical shadow radius

This section explores the correlation between the shadow and Quasinormal Modes (QNMs). QNMs are well-recognized as modes associated with the ringdown phase of a black hole. They may be expressed in terms of their real and imaginary components, denoted $\Sigma = \Sigma_r - i\,\Sigma_i$. Here, Σ_r and Σ_i are respectively denoting the real and imaginary QNMs. A recent

argument has been made about the relationship between the shadow radius and the real component of QNMs for static metrics, as [90,91]

$$R_s = \frac{\Omega + \frac{1}{2}}{\Sigma_r}. \tag{59}$$

In Eq. 59, Ω represents angular momentum of the perturbation. It was shown in Ref. [92] that the Kerr black hole's QNM frequency in the eikonal limit reads,

$$\Sigma_Q = \left(\Omega + \frac{1}{2}\right)\omega_r - i\sigma\left(n + \frac{1}{2}\right), \tag{60}$$

where n is the overtone number and

$$\omega_r = \omega_\theta + \frac{m}{\Omega + \frac{1}{2}}\omega_{pre}. \tag{61}$$

The symbol ω_θ represents the orbital frequency in the polar direction. Furthermore, ω_{pre} specifies the Lense–Thiring precision frequency of the orbit plane, while σ represents the orbit's Lyapunov exponent. In the following part, we examine the relationship between QNMs and the shadow radius observed by an observer at a significant distance from the black hole. It is well known that rotation distorts the black hole shadow; as a consequence, the form of the shadow varies with the viewing angle. In the following, we will look at two separate cases.

5.1 For $\theta_0 = \frac{\pi}{2}$

Typically, there is no specific term for the shadow [93]. However, for the sake of this discussion, we will focus on the scenario when $\theta_0 = \frac{\pi}{2}$. To simplify matters, we will additionally consider the equatorial orbit, which may be used to calculate the standard shadow radius. In addition, we will utilize the fact that the Lense–Thirring precession frequency is connected to the orbital frequency and the Keplerian frequency. Specifically, the Lense–Thirring precession frequency for orbits that rotate in the same direction as the perturbation, with a small deviation from the equatorial plane, can be expressed as follows [94]:

$$\omega_{pre} = \pm\omega_\phi \mp \omega_\theta \tag{62}$$

where

$$\omega_\phi = \frac{-\partial_r g_{t\phi} \pm \sqrt{(\partial_r g_{t\phi})^2 - (\partial_r g_{tt})(\partial_r g_{\phi\phi})}}{\partial_r g_{\phi\phi}}. \tag{63}$$

The WKB analysis method may be used to examine Kerr QNMs by representing the integral $2\int_{\theta_-}^{\theta_+}\sqrt{\Theta}d\theta$ as $2\pi(L - |L_Q|)$, which can be interpreted as the Bohr-Sommerfeld Condition. This may be linked to the eigenvalue problem in the θ direction for the Kerr QNMs (see Ref. [92] for more information). There was a debate over

$$\kappa + L^2 \simeq L_Q^2 - \frac{a^2E^2}{2}\left(1 - \frac{L^2}{L_Q^2}\right). \tag{64}$$

Upon simplification of the equation mentioned above, we get

$$\xi + \eta^2 \simeq \frac{L_Q^2}{E^2} - \frac{a^2}{2}\left(1 - \frac{L^2}{L_Q^2}\right). \tag{65}$$

Now, as stated in Reference [92], we possess

$$\begin{aligned} L &\longleftrightarrow m \\ E &\longleftrightarrow \Sigma_r \\ L_Q &\longleftrightarrow \Omega + \frac{1}{2}. \end{aligned} \tag{66}$$

The equation $\Sigma_r = L_Q\omega_r$ is stated here. In the Eikonal limit, when $m = \Omega >> 1$, we find that $\nu = m/(\Omega + 1/2) = 1$, in addition to

$$\omega_{pre} = \omega_\phi - \omega_\theta. \tag{67}$$

Therefore, we have,

$$\omega_r = \omega_\theta + \omega_{pre} = \omega_\phi. \tag{68}$$

To better understand, these Quasi-Normal Modes (QNMs) are associated with the Kepler frequency, as stated in the Ref. [93].

$$\Sigma_r^\pm = \left(\Omega + \frac{1}{2}\right) \times \frac{-\partial_r g_{t\phi} \pm \sqrt{(\partial_r g_{t\phi})^2 - (\partial_r g_{tt})(\partial_r g_{\phi\phi})}}{\partial_r g_{\phi\phi}}, \tag{69}$$

where $1 << \Omega = m$. Now, for the shadow radius, we have

$$\bar{R}_s = \frac{1}{2}\left(\alpha^+(r_p^+) - \alpha^-(r_p^-)\right). \tag{70}$$

here $\alpha^\pm(r_p) = \pm\sqrt{f(r_0)}\eta$ and $\xi(r_p^\pm) = 0$. Now from Eq.(65) we have,

$$\eta^\pm = \pm\sqrt{\frac{(\Omega + \frac{1}{2})^2}{\Sigma_r^2(r_p^\pm)} - \frac{a^2}{2}(1 - \nu^2)}. \tag{71}$$

Therefore, we have [94].

$$\bar{R}_s = \frac{\sqrt{f(r_0)}}{2}\sqrt{\frac{(\Omega + \frac{1}{2})^2}{\Sigma_r^2(r_p^+)} - \frac{a^2}{2}(1 - \nu^2)} + \frac{\sqrt{f(r_0)}}{2}\sqrt{\frac{(\Omega + \frac{1}{2})^2}{\Sigma_r^2(r_p^-)} - \frac{a^2}{2}(1 - \nu^2)}. \tag{72}$$

The symbol r_0 denotes the position of the observer. Now, for the eikonal limit if we set $m = \pm\Omega$ (i.e. $\nu = \pm 1$), we have [95]

$$\bar{R}_s(\nu = \pm 1) = \left(\Omega + \frac{1}{2}\right)$$

$$\times \frac{\sqrt{f(r_0)}}{2}\left(\frac{1}{\Sigma_r(r_p^+)}-\frac{1}{\Sigma_r(r_p^-)}\right). \tag{73}$$

The static case occurs when $\Sigma_r^+ = \Sigma_r^- = \Sigma_r$. Therefore, we possess

$$\bar{R}_s = \sqrt{f(r_0)}\frac{\Omega+\frac{1}{2}}{\Sigma_r}. \tag{74}$$

By using algebraic methods in the geometric limit and metric functions, it is possible to make Eq. (69) easier to understand, as shown in Ref. [93]. Making this simpler as

$$\Sigma_r^{\pm} = \left(\Omega+\frac{1}{2}\right) - \frac{1}{a \pm \sqrt{\frac{2r_p^{\pm}}{f'(r)|_{r_p^{\pm}}}}}. \tag{75}$$

It is possible to simplify the typical shadow radius equation to acquire a more concise expression, as the following:

$$\bar{R}_s = \frac{\sqrt{2f(r_0)}}{2}\left(\sqrt{\frac{r_p^+}{f'(r)|_{r_p^+}}}+\sqrt{\frac{r_p^-}{f'(r)|_{r_p^-}}}\right). \tag{76}$$

The above equation is the same as the one found in a prior Ref. [92], where $r_p^{\pm}$ values can be found by solving [93],

$$r_p^2 - \frac{2r_p}{f'(r)|_{r_p^{\pm}}}f(r_p) \mp 2a\sqrt{\frac{2r_p}{f'(r)|_{r_p^{\pm}}}} = 0. \tag{77}$$

5.2 For $\theta_0 = 0$ and π

Let's examine the polar orbit where $\theta = 0$. In this scenario, it is appropriate to calculate the observer's viewing angle, denoted as θ_0, for two cases: when $\theta_0 = 0$ and $\theta_0 = \pi$. The polar orbit lacks azimuthal angular momentum, leading to a $L = 0$ value. By considering the circular geodesics, it can be shown that

$$(a^2+r^2)^2 - R_p^2(a^2+r^2f(r)) = 0, \tag{78}$$

and

$$(a^2+r^2)4r - 2rR_p^2f(r) - r^2R_p^2f'(r) = 0. \tag{79}$$

It is important to mention that in this particular situation, R_p denotes the impact parameter and is defined as $R_p = a^2 + \kappa/E^2$ [96]. Now, using Eq. (78), we may infer

$$R_p^{\pm} = \pm\frac{r^2+a^2}{\sqrt{a^2+r^2f(r)}}_{r_p}. \tag{80}$$

Using the given specification $\bar{R}_s := (1/2)(\sqrt{f(r_0)}R_p^+ - \sqrt{f(r_0)}R_p^-$, the formula for the shadow radius may be based on the reference [94].

$$\bar{R}_s = \sqrt{f(r_0)}\frac{r^2+a^2}{\sqrt{a^2+r^2f(r)}}\Big|_{r_p}. \tag{81}$$

To get the values of r_p in this situation, one may use the following equation:

$$(r_p^2+a^2)^2 - \frac{4(r_p^2+a^2)(a^2+r_p^2f(r_p))}{2f(r_p)+r_pf'(r_p)} = 0. \tag{82}$$

Given that $L = 0$ and based on Eq. (63), the shadow radius may be calculated as

$$\bar{R}_s = \sqrt{f(r_0)}\sqrt{\frac{(\Omega+\frac{1}{2})^2}{\Sigma_r^2(r_p)}+\frac{a^2}{2}}. \tag{83}$$

As anticipated, it is straightforward to ascertain that the shadow radius decreases to the value specified in Eq. (73) when there is no rotation. By combining Eqs. (73) and (80), we may represent the real component of Quasi-Normal Modes (QNMs) as follows,

$$\Sigma_r = \sqrt{\frac{2\left(a^2+r^2f(r)\right)}{2(r^2+a^2)^2-(a^2+r^2f(r))a^2}}\left(\Omega+\frac{1}{2}\right)\Big|_{r=r_p}. \tag{84}$$

The corresponding numerical values of equatorial (first and second row) and polar (third row) QNMs have been documented in Table 1. As the value of Ω increases, we anticipate that the frequency of the QNMs will be more precisely identified.

6 Conclusion

Theoretical studies of black hole shadows and recent EHT observations have opened new possibilities for testing gravity theories and obtaining constraints on their parameters. This work has focused on photon motion and the shadow of charged rotating black holes in EMS theory. In the first step, we obtained a rotating charged black hole solution in EMS gravity using NJA and investigated the structure of the event horizon of the rotating black hole in EMS theory, as described by the metric (30), we proceed by solving the equation $g^{rr} = 0$ to obtain the roots that correspond to the radius of the horizon.

We have demonstrated that an increase in the parameter β, with $\gamma = 0$, significantly increases the extreme value of the charge Q. In contrast, the limiting value of Q decreases with an increase of β when γ is negative. In addition, there are noticeable distinctions between the scenarios of positive and negative values of the parameter γ.

In specific parameter configurations, a black hole might possess a single horizon. For example, setting $\gamma = 0$ and $\beta = 0.5$, a black hole exhibits a single horizon at $a/M = 0.8$ and $Q/M = 0.85$. A subsequent increase in Q/M leads to the disappearance of the black hole's horizon. In light of these characteristics, it is possible to formulate an expression for

Table 1 Numerical values of the real part of QNMs for equatorial modes and polar mode at $M = 1$, $Q = 0.1$, $\beta = 0.25$, $a = 0.5$, $\gamma = 0.5$ and $r = r_p$

Ω	1	2	3	4	5	6	7	8	9	10
Σ_r^+	1.35987	2.35987	3.35987	4.35987	5.35987	6.35987	7.35987	8.hl35987	9.35987	10.3599
Σ_r^-	1.82327	2.82327	3.82327	4.82327	5.82327	6.82327	7.82327	8.82327	9.82327	10.8233
Σ_r	0.293771	0.489618	0.685465	0.881313	1.07716	1.27301	1.46885	1.6647	1.86055	2.0564

the maximum spin that distinguishes between a black hole and a naked singularity.

The geodesic structure near the rotating black hole within the EMS theory, as outlined by Eq. (30), has been subject to investigation. We examined the circular photon orbits around the black hole by evaluating the effective potential, a pivotal parameter for studying the shadow generated by the rotating black hole. The geodesic equations were derived using the HJ method. Subsequently, we obtained the effective potential governing the circular motion of photons in the spacetime of the rotating black hole along null geodesic lines.

The investigation of the shadow cast by a rotating black hole in the EMS theory involved exploring various parameter ranges, including a, Q, β, and γ. The findings revealed that the size of the shadow is contingent on the black hole parameters. As the Q parameter increases, the shadow region decreases in size, and the shape of the shadow becomes more distorted, particularly as Q/M approaches unity. Furthermore, the shadow area experiences a reduction with a growth in the parameter β, while the shadow radius expands with an increase in the value of γ.

Indeed, the silhouette of a black hole serves as a unique manifestation of the features of the black hole spacetime. To achieve constraints on spacetime parameters, it is essential to define measurable variables, namely the shape and size of the shadow. We have shown that the shadow area A decreases with increasing a and Q, while the shadow area expands as γ increases. Likewise, the oblateness D decreases with an augmentation in the spin and charge parameters and increases under the influence of the parameter γ. Furthermore, the parameter β reduces the area and the oblateness values.

Finally, we have investigated rotating black holes M87* and Sgr A* within the framework of the EMS theory to contrast the theoretical results derived from shadow analysis with the shadow images of M87* and Sgr A* observed by the EHT. Our analysis of density plots has shown that the upper limit of the charge parameter Q increases as the fixed value of the parameter β decreases. The maximum value of Q increases from around $0.58M$ to more than $0.7M$. However, there is a significant difference between the results when the parameter γ has different values. In addition, the angular diameter varies across the $a - Q$ space as the inclination angle changes. Ultimately, we identified and examined standard shadow radius, equatorial, and polar QNMs using the geometric-optic link between QNM parameters and conserved values along geodesics. As Ω increases, it is observed that the frequency of QNMs is more accurately recognized.

Acknowledgements This research is supported by Grants No. F-FA-2021-510 and FZ-20200929385 of the Ministry of Higher Education, Science, and Innovations of the Republic of Uzbekistan.

Data Availability Statement This manuscript has no associated data. [Author's comment: Data sharing does not apply to this article as no datasets were generated or analyzed during the current study.]

Code Availability Statement This manuscript has no associated code/software. [Author's comment: Code/Software sharing does not apply to this article as no code/software was generated or analyzed during the current study.]

Funded by SCOAP[3].

References

1. G.W. Gibbons, K.I. Maeda, Nucl. Phys. B **298**(4), 741 (1988). https://doi.org/10.1016/0550-3213(88)90006-5
2. D. Garfinkle, G.T. Horowitz, A. Strominger, Phys. Rev. D **43**(10), 3140 (1991). https://doi.org/10.1103/PhysRevD.43.3140
3. D. Brill, G.T. Horowitz, Phys. Lett. B **262**(4), 437 (1991). https://doi.org/10.1016/0370-2693(91)90618-Z
4. R. Gregory, J.A. Harvey, Phys. Rev. D **47**(6), 2411 (1993). https://doi.org/10.1103/PhysRevD.47.2411
5. T. Koikawa, M. Yoshimura, Phys. Lett. B **189**(1–2), 29 (1987). https://doi.org/10.1016/0370-2693(87)91264-0
6. D.G. Boulware, S. Deser, Phys. Lett. B **175**(4), 409 (1986). https://doi.org/10.1016/0370-2693(86)90614-3
7. M. Rakhmanov, Phys. Rev. D **50**(8), 5155 (1994). https://doi.org/10.1103/PhysRevD.50.5155

8. B. Harms, Y. Leblanc, Phys. Rev. D **46**(6), 2334 (1992). https://doi.org/10.1103/PhysRevD.46.2334
9. C.F.E. Holzhey, F. Wilczek, Nucl. Phys. B **380**(3), 447 (1992). https://doi.org/10.1016/0550-3213(92)90254-9
10. Z. Stuchlík, M. Kološ, J. Kovář, P. Slaný, A. Tursunov, Universe **6**(2), 26 (2020). https://doi.org/10.3390/universe6020026
11. J.M. Maldacena, Adv. Theor. Math. Phys. **2**, 231 (1998)
12. J. Maldacena, Int. J. Theor. Phys. **38**, 1113 (1999). https://doi.org/10.1023/A:1026654312961
13. E. Witten, Adv. Theor. Math. Phys. **2**, 253 (1998)
14. D. Klemm, W.A. Sabra, Phys. Lett. B **503**(1–2), 147 (2001). https://doi.org/10.1016/S0370-2693(01)00181-2
15. S.S. Gubser, I.R. Klebanov, A.M. Polyakov, Phys. Lett. B **428**(1–2), 105 (1998). https://doi.org/10.1016/S0370-2693(98)00377-3
16. O. Aharony, S.S. Gubser, J. Maldacena, H. Ooguri, Y. Oz, Phys. Rep. **323**(3), 183 (2000). https://doi.org/10.1016/S0370-1573(99)00083-6
17. P. Jai-akson, A. Chatrabhuti, O. Evnin, L. Lehner, Phys. Rev. D **96**(4), 044031 (2017). https://doi.org/10.1103/PhysRevD.96.044031
18. M. Heydari-Fard, M. Heydari-Fard, H.R. Sepangi, Eur. Phys. J. C **80**(4), 351 (2020). https://doi.org/10.1140/epjc/s10052-020-7911-0
19. B. Turimov, J. Rayimbaev, A. Abdujabbarov, B. Ahmedov, Z. Stuchlík, Phys. Rev. D **102**(6), 064052 (2020). https://doi.org/10.1103/PhysRevD.102.064052
20. M. Zahid, J. Rayimbaev, S.U. Khan, J. Ren, S. Ahmedov, I. Ibragimov, Eur. Phys. J. C **82**(5), 494 (2022). https://doi.org/10.1140/epjc/s10052-022-10432-8
21. N. Kurbonov, J. Rayimbaev, M. Alloqulov, M. Zahid, F. Abdulxamidov, A. Abdujabbarov, M. Kurbanova, Eur. Phys. J. C **83**(6), 506 (2023). https://doi.org/10.1140/epjc/s10052-023-11691-9
22. J. Rayimbaev, A. Abdujabbarov, F. Abdulkhamidov, V. Khamidov, S. Djumanov, J. Toshov, S. Inoyatov, Eur. Phys. J. C **82**(12), 1110 (2022). https://doi.org/10.1140/epjc/s10052-022-11080-8
23. V. Perlick, O.Y. Tsupko, Phys. Rep. **947**, 1 (2022)
24. S. Chen, J. Wang, Int. J. Mod. Phys. D **25**(12), 1650041 (2016)
25. S. Vagnozzi et al., Phys. Rev. D **100**(2), 024020 (2020)
26. R. Kumar, S.G. Ghosh, Astrophys. J. **892**(1), 78 (2020)
27. S.W. Wei, Y.X. Liu, J. Cosmol. Astropart. Phys. **2013**(11), 063 (2013)
28. P.V.P. Cunha, C.A.R. Herdeiro, Gen. Relativ. Gravit. **50**(4), 42 (2018)
29. K. Akiyama et al., Astrophys. J. Lett. **875**, L1 (2019). https://doi.org/10.3847/2041-8213/ab0ec7
30. T. Johannsen, D. Psaltis, Astrophys. J. **718**, 446 (2010). https://doi.org/10.1088/0004-637X/718/1/446
31. L. Rezzolla, A. Zhidenko, Phys. Rev. D **90**(8), 084009 (2014). https://doi.org/10.1103/PhysRevD.90.084009
32. R. Konoplya, L. Rezzolla, A. Zhidenko, Phys. Rev. D **93**(6), 064015 (2016). https://doi.org/10.1103/PhysRevD.93.064015
33. H. Falcke, F. Melia, E. Agol, Astrophys. J. Lett. **528**, L13 (2000). https://doi.org/10.1086/312423
34. J.L. Synge, Mon. Not. R. Astron. Soc. **131**(3), 463 (1966). https://doi.org/10.1093/mnras/131.3.463
35. K. Akiyama et al., Astrophys. J. Lett. **875**(1), L2 (2019). https://doi.org/10.3847/2041-8213/ab0c96
36. K. Akiyama et al., Astrophys. J. Lett. **875**(1), L3 (2019). https://doi.org/10.3847/2041-8213/ab0c57
37. K. Akiyama et al., Astrophys. J. Lett. **875**(1), L5 (2019). https://doi.org/10.3847/2041-8213/ab0f43
38. K. Akiyama et al., Astrophys. J. Lett. **875**(1), L6 (2019). https://doi.org/10.3847/2041-8213/ab1141
39. K. Akiyama et al., Astrophys. J. Lett. **930**(2), L12 (2022). https://doi.org/10.3847/2041-8213/ac6674
40. K. Akiyama et al., Astrophys. J. Lett. **930**(2), L15 (2022). https://doi.org/10.3847/2041-8213/ac6736
41. K. Akiyama et al., Astrophys. J. Lett. **930**(2), L17 (2022). https://doi.org/10.3847/2041-8213/ac6756
42. V. Cardoso, P. Pani, Living Rev. Relativ. **22**(1), 4 (2019). https://doi.org/10.1007/s41114-019-0020-4
43. M. Zahid, S.U. Khan, J. Ren, J. Rayimbaev, Int. J. Mod. Phys. D **31**(08), 2250058 (2022)
44. M. Zahid, F. Sarikulov, C. Shen, J. Rayimbaev, K. Badalov, S. Muminov, Chin. J. Phys. **91**, 45 (2024)
45. M. Zahid, F. Sarikulov, C. Shen, M. Umaraliyev, J. Rayimbaev, Phys. Dark Universe **46**, 101616 (2024)
46. S.U. Khan, J. Ren, Phys. Dark Universe **30**, 100644 (2020)
47. S.U. Khan, J. Ren, Chin. J. Phys. **78**, 141 (2022)
48. M. Zubair, M.A. Raza, G. Abbas, Eur. Phys. J. C **82**(10), 948 (2022)
49. M. Zubair, M.A. Raza, F. Sarikulov, J. Rayimbaev, J. Cosmol. Astropart. Phys. **2023**(10), 058 (2023)
50. M. Zubair, M.A. Raza, E. Maqsood, Phys. Dark Universe **42**, 101334 (2023)
51. M.A. Raza, J. Rayimbaev, F. Sarikulov, M. Zubair, B. Ahmedov, Z. Stuchlík, Phys. Dark Universe **44**, 101488 (2024)
52. R. Shaikh, Mon. Not. R. Astron. Soc. **523**(1), 375 (2023). https://doi.org/10.1093/mnras/stad1383
53. Y. Guo, C. Lan, Y.G. Miao, (2022). https://doi.org/10.48550/arXiv.2201.02971. arXiv e-prints arXiv:2201.02971
54. N. Tsukamoto, Phys. Rev. D **105**(8), 084036 (2022). https://doi.org/10.1103/PhysRevD.105.084036
55. J. Zhang, Y. Xie, Eur. Phys. J. C **82**(5), 471 (2022). https://doi.org/10.1140/epjc/s10052-022-10441-7
56. M.S. Churilova, Z. Stuchlík, Ann. Phys. **418**, 168181 (2020). https://doi.org/10.1016/j.aop.2020.168181
57. N. Tsukamoto, Phys. Rev. D **104**(6), 064022 (2021). https://doi.org/10.1103/PhysRevD.104.064022
58. S.U. Islam, J. Kumar, S.G. Ghosh, J. Cosmol. Astropart. Phys. **2021**(10), 013 (2021). https://doi.org/10.1088/1475-7516/2021/10/013
59. J. Zhang, Y. Xie, Eur. Phys. J. C **82**(10), 854 (2022). https://doi.org/10.1140/epjc/s10052-022-10846-4
60. J. Rayimbaev, R.C. Pantig, A. Övgün, A. Abdujabbarov, D. Demir, Ann. Phys. **454**, 169335 (2023). https://doi.org/10.1016/j.aop.2023.169335
61. B. Puliçe, R.C. Pantig, A. Övgün, D. Demir, Class. Quantum Gravity **40**(19), 195003 (2023). https://doi.org/10.1088/1361-6382/acf08c
62. S. Vagnozzi, R. Roy, Y.D. Tsai, L. Visinelli, M. Afrin, A. Allahyari, P. Bambhaniya, D. Dey, S.G. Ghosh, P.S. Joshi, K. Jusufi, M. Khodadi, R.K. Walia, A. Övgün, C. Bambi, Class. Quantum Gravity **40**(16), 165007 (2023). https://doi.org/10.1088/1361-6382/acd97b
63. A. Uniyal, R.C. Pantig, A. Övgün, Phys. Dark Universe **40**, 101178 (2023). https://doi.org/10.1016/j.dark.2023.101178
64. R.C. Pantig, A. Övgün, Ann. Phys. **448**, 169197 (2023). https://doi.org/10.1016/j.aop.2022.169197
65. F. Atamurotov, U. Papnoi, K. Jusufi, Class. Quantum Gravity **39**(2), 025014 (2022). https://doi.org/10.1088/1361-6382/ac3e76
66. E. Ghorani, B. Puliçe, F. Atamurotov, J. Rayimbaev, A. Abdujabbarov, D. Demir, Eur. Phys. J. C **83**(4), 318 (2023). https://doi.org/10.1140/epjc/s10052-023-11490-2
67. S. Yu, J. Qiu, C. Gao, (2020). arXiv e-prints arXiv:2005.14476
68. E.T. Newman, A.I. Janis, J. Math. Phys. **6**(6), 915 (1965). https://doi.org/10.1063/1.1704350
69. E.T. Newman, E. Couch, K. Chinnapared, A. Exton, A. Prakash, R. Torrence, J. Math. Phys. **6**(6), 918 (1965). https://doi.org/10.1063/1.1704351
70. M. Azreg-Aïnou, Phys. Rev. D **90**, 064041 (2014). https://doi.org/10.1103/PhysRevD.90.064041

71. M. Azreg-Aïnou, Eur. Phys. J. C **74**, 2865 (2014). https://doi.org/10.1140/epjc/s10052-014-2865-8
72. M. Fathi, M. Olivares, J.R. Villanueva, Galaxies **9**(2) (2021). https://www.mdpi.com/2075-4434/9/2/43
73. R.K. Walia, S.D. Maharaj, S.G. Ghosh, Eur. Phys. J. C **82**(6), 547 (2022). https://doi.org/10.1140/epjc/s10052-022-10451-5
74. U. Papnoi, F. Atamurotov, Phys. Dark Universe **35**, 100916 (2022). https://doi.org/10.1016/j.dark.2021.100916
75. J.M. Bardeen, in *Black Holes (Les Astres Occlus)* (1973), Gordon and Breach, New York, pp. 215–239
76. K. Hioki, K.I. Maeda, Phys. Rev. D **80**, 024042 (2009). https://doi.org/10.1103/PhysRevD.80.024042
77. J. Schee, Z. Stuchlík, Int. J. Mod. Phys. D **18**(6), 983 (2009). https://doi.org/10.1142/S0218271809014881
78. M. Amir, S.G. Ghosh, Phys. Rev. D **94**, 024054 (2016). https://doi.org/10.1103/PhysRevD.94.024054
79. A.A. Abdujabbarov, L. Rezzolla, B.J. Ahmedov, Mon. Not. R. Astron. Soc. **454**(3), 2423 (2015). https://doi.org/10.1093/mnras/stv2079
80. R. Kumar, S.G. Ghosh, Astrophys. J. **892**, 78 (2020). https://doi.org/10.3847/1538-4357/ab77b0
81. F. Sarikulov, F. Atamurotov, A. Abdujabbarov, B. Ahmedov, Eur. Phys. J. C **82**(9), 771 (2022). https://doi.org/10.1140/epjc/s10052-022-10711-4
82. E. Teo, Gen. Relativ. Gravit. **53**(1), 10 (2021). https://doi.org/10.1007/s10714-020-02782-z
83. K. Jusufi, M. Azreg-Aïnou, M. Jamil, E.N. Saridakis, Universe **8**(2), 102 (2022). https://doi.org/10.3390/universe8020102
84. M. Okyay, A. Övgün, JCAP **01**(01), 009 (2022). https://doi.org/10.1088/1475-7516/2022/01/009
85. M. Afrin, R. Kumar, S.G. Ghosh, Mon. Not. R. Astron. Soc. **504**, 5927 (2021). https://doi.org/10.1093/mnras/stab1260
86. Y. Chen, R. Roy, S. Vagnozzi, L. Visinelli, Phys. Rev. D **106**(4), 043021 (2022). https://doi.org/10.1103/PhysRevD.106.043021
87. M. Afrin, S. Vagnozzi, S.G. Ghosh, Astrophys. J. **944**(2), 149 (2023). https://doi.org/10.3847/1538-4357/acb334
88. M. Zahid, J. Rayimbaev, F. Sarikulov, S.U. Khan, J. Ren, Eur. Phys. J. C **83**(9), 855 (2023). https://doi.org/10.1140/epjc/s10052-023-12025-5
89. M. Zubair, M.A. Raza, F. Sarikulov, J. Rayimbaev, J. Cosmol. Astropart. Phys. **2023**(10), 34 (2023)
90. K. Jusufi, Phys. Rev. D **101**(12), 124063 (2020)
91. B. Cuadros-Melgar, R. Fontana, J. de Oliveira, Phys. Lett. B **811**, 135966 (2020)
92. H. Yang, D.A. Nichols, F. Zhang, A. Zimmerman, Z. Zhang, Y. Chen, Phys. Lett. D **86**(10), 104006 (2012)
93. K. Jusufi, M. Azreg-Aïnou, M. Jamil, Q. Wu, Universe **8**(4), 210 (2022)
94. F. Atamurotov, I. Hussain, G. Mustafa, K. Jusufi, Eur. Phys. J. C **82**(9), 1 (2022)
95. V. Cardoso, A.S. Miranda, E. Berti, H. Witek, V.T. Zanchin, Phys. Rev. D **79**(6), 064016 (2009)
96. S.R. Dolan, Phys. Rev. D **82**(10), 104003 (2010)